BMC Plant Biology

RESEARCH

Open Access

ROS homeostasis and cell wall biosynthesis pathway are involved in female inflorescence development of birch (*Betula platyphylla*)

Mengjie Cai[1†], Kehao Zeng[1†], Lanlan Li[1], Jiayuan Shi[1], Bello Hassan Jakada[1], Xue Zhang[1], Pu Wang[1], Haonan Zhu[1], Jing Jiang[2] and Xingguo Lan[1*]

Abstract

Background Female inflorescence development from megasporogenesis to gametogenesis, and mature female gametophyte (FG), is a complex and important event in plant sexual reproduction. However, how this essential developmental process is regulated in birch remains obscure. This study conducted extensive morphological and transcriptomic analyses to reveal possible regulatory mechanisms during birch female inflorescence development.

Results Histological analyses showed that birch exhibits a Polygonum-type embryo sac. During early ovule development, the ovule primordium emerges and subsequently differentiates into the archesporial cell (ASC), initiating megasporogenesis. The megaspore mother cell (MMC) then undergoes meiosis, generating a functional megaspore (FM) that develops into the mature embryo sac (MES). Transcriptomic profiling revealed upregulation of reactive oxygen species (ROS)-scavenging genes, including *BpGSTU17*, *BpGSTU19*, *BpAPX1*, *BpPRXIIE*-1, *BpSODCP*, and *BpFDX3*, at the MMC stage. At the MES stage, genes involved in both ROS synthesis and scavenging, such as *BpACX*, *BpCuAOγ1*, *BpGLO1*, *BpRBOHH*, *BpUOX2*, *BpFSD2*, *BpCAT3*, *BpGRX*, *BpNRX*, and *BpTRX*, were significantly expressed. *BpPAL*, *BpC4H*, *BpCSE*, *BpCoMT*, *BpCCoAOMT*, *BpCAD*, *BpF5H*, *BpLAC*, *BpXTH23*, and *BpCESA*, genes involved in the cell wall biosynthesis pathways including lignin, cellulose, hemicellulose and pectin, were also upregulated.

Conclusion Our results suggest that ROS homeostasis affects the process of birch megasporogenesis. Genes related to ROS signaling and cell wall synthesis participate in embryo sac maturation.

Keywords Birch, Female inflorescence, Transcriptome, Reactive oxygen species, Cell wall biosynthesis

[†]Mengjie Cai and Kehao Zeng these authors contributed equally.

*Correspondence:
Xingguo Lan
lanxingguo@nefu.edu.cn
[1]Key Laboratory of Saline-Alkali Vegetation Ecology Restoration, Northeast Forestry University, Harbin 150040, Heilongjiang, China
[2]State Key Laboratory of Tree Genetics and Breeding, Northeast Forestry University, Harbin 150040, Heilongjiang, China

Introduction

Angiosperm embryo sacs take many forms, and most species have a polygonum-type embryo sac [1], which usually consists of two developmental stages: megasporogenesis and gametogenesis [2]. Megasporogenesis comprises three developmental phases, namely the archesporial cell (ASC), themegaspore mother cell (MMC), and the functional megaspore (FM). It then passes through three nuclear division cycles, followed by nuclear migration, polar nuclear fusion, and cellularization, ultimately forming a mature embryo sac (MES) [3, 4]. The female gametophyte (FG) development is a complex and tightly regulated process. Genes involved with signal transduction and structural specification are implicated in the formation of FG [5–7].

The ROS (reactive oxygen species) signaling network is a key element for plant stress signal transduction. ROS are a pervasive by-product of aerobic metabolism and were initially reported only as harmful oxidants causing permanent oxidative damage to biomacromolecules [8, 9]. However, there is growing evidence that ROS regulate biological processes such as development, stress tolerance, plant immunity, cell fate determination, and pollination [10–14]. The mechanisms by which ROS regulates key growth processes have been reported in plants, animals, and even fungi [15–17]. Several ROS molecules exhibit unique characteristics in terms of reaction preference, kinetics, production sites, and degradation [18]. The superoxide ($O_2^{\bullet-}$) and hydrogen peroxide (H_2O_2) are the most important among the biologically relevant and abundant ROS molecules [19]. ROS function as signaling molecules that use steady states and concentration oscillations to control physiological activities. Thus, a highly dynamic ROS signaling network is essential for maintaining normal plant developmental processes [20, 21]. Myriad antioxidative regulatory systems exist in the cell to keep ROS at a minimum toxic level, and any change in the balance could trigger ROS signaling reactions [22].

Effective ROS signaling relies on transient elevation of ROS concentrations that remain strictly below cytotoxic thresholds [23]. Respiratory burst oxidase homologs (RBOHs) function as central regulators of ROS signaling, mediating localized ROS bursts, such as RBOH-dependent superoxide anion ($O_2^{\bullet-}$) production during gametophyte development to orchestrate cellular communication [21, 24, 25]. Genomic analyses in birch have identified polyamine oxidase (PAO) family members, which contribute to H_2O_2 biosynthesis [26]. Other enzymatic systems involved in ROS generation include acyl-CoA oxidase (ACX), copper amine oxidase (CuAO), urate oxidase (UOX), and glycolate oxidase (GOX). Plants maintain ROS homeostasis through a multilayered antioxidant network, Superoxide dismutase (SOD) catalyzes the conversion of $O_2^{\bullet-}$ to H_2O_2 and O_2, mitigating ROS cytotoxicity and supporting female gametophyte development [27]. The ascorbate-glutathione (AsA-GSH) cycle coordinates ascorbate peroxidase (APX) and glutathione peroxidase (GPX) activities to scavenge H_2O_2, a critical pathway in stress response regulation [28, 29]. Peroxiredoxins (PRXs) utilize H_2O_2 as an oxidant to drive redox reactions across diverse substrates, participating in developmental processes, cell wall dynamics, and environmental stress adaptation [30]. Glutathione S-transferases (GSTs) detoxify ROS via glutathione conjugation while modulating auxin/jasmonate signaling and programmed cell death [31]. Additionally, ROS production is regulated by other factors; for instance, mitogen-activated protein kinase kinase 3 (MKK3) suppresses the expression of RBOH through the MAP kinase phosphorylation cascade [32].

Cell wall biosynthesis is an important part of structural specification. There have been many studies on the involvement of cell wall-related genes in gametophyte development. To our knowledge, however, little is yet reported about the involvement of the cell wall biosynthesis pathway in FG development. Plant cells need the mechanical support of cell walls to grow, develop, and adapt to their changing surroundings. Cell wall plasticity is a concise description of the capacity for their dynamic change. Dynamic changes in the synthesis levels of polysaccharides such as lignin, cellulose, hemicellulose and pectin are the source of cell wall plasticity [33]. Lignin is reported to be derived from phenylalanine and represents a cell wall structural component in vascular plants. Lignin serves as a diffusion barrier, a structural support system, and a defense against environmental stress for plant cells [34]. Cellulose serves as the primary structural scaffold of the cell wall, with cellulose synthase A (CESA) catalyzing the biosynthesis of cellulose [35]. Mutants of the *CESA* gene exhibit phenotypes with significantly reduced cellulose content and primary/secondary wall thicknesses [36, 37]. It is noteworthy that it has been reported that although several CESA proteins exist in the same cell type, mutation in any *CESA* genes is sufficient to cause cellulose reduction [38]. Xyloglucan is the most common hemicellulose in dicotyledonous plants and is found in many monocotyledonous plants [39]. The xyloglucan endotransglucosylase/hydrolases (XTHs) are key enzymes for xyloglucan synthesis [40]. Xyloglucan affects plant growth and development mainly by regulating cell wall rigidity. Another class of cell wall components includes pectin, with the polysaccharide galacturonic acid being an essential component of pectin, with polysaccharide galacturonic acid being one of the main components of pectin. Pectic polysaccharides control the porosity and extensibility during cell morphogenesis. Homogalacturonan (HG) is the most abundant pectin subtype in plants [41]. The α-1,4-galacturonosyltransferase (GAUT) is the

enzyme that produces HG [42]. Pectin methylesterases (PMEs) eliminate the methyl-ester from unbranched HG, and pectin methylesterase inhibitor(PMEIs) have an antagonistic inhibitory effect on this activity. They influence the biochemical properties of pectin, which impacts the makeup and function of cell walls for plant growth and development [43]. Many enzymes or transcription factors such as polygalacturonase 4 (PGLR4) and MYB52 work together to regulate the degree of methyl esterification of pectin [44, 45].

In this study, we characterized the development of birch female inflorescences after pollination. In addition, we performed transcriptome analyses on samples from the MMC, FM, and MES stages. Our results showed that genes regulating ROS homeostasis and cell wall formation were specifically expressed at distinct stages of female inflorescence development, suggesting that they could be important female inflorescence regulators.

Materials and methods

Plant material

Birch (*Betula platyphylla*) female inflorescences were collected from the breeding site of the Northeast Forestry University State Key Laboratory of Tree Genetics and Breeding (latitude 45° 43′, longitude 126° 38′). To systematically assess the developmental stages of the female inflorescences, post-pollination samples at 0 days after pollination (DAP) were collected, followed by daily collections of post-pollination inflorescence at a consistent time point, starting from 1 DAP and continuing up to 50 DAP.

Histological analyses

The female inflorescence at different stages were selected for histological analyses. The samples were subjected to gentle vacuum infiltration in Formalin-Aceto-Alcohol (FAA) fixative containing 70% ethanol; 37% acetic acid; and formaldehyde 18% for about 5 h and moved to 4 °C overnight. The pistil was carefully separated using a dissecting needle under a dissection microscope and dehydrated through a gradient of 50%, 70%, 85%, and 100% ethanol for 1 h in each stage. After the sample was dehydrated, it was gradually replaced with 100% ethanol with xylene through a series of xylene: ethanol mixtures. The replacement was conducted in the ratios: 1:1, 7:3, 17:3, and finally pure xylene, with each step lasting for 1 h. Xylene in the samples was gradually replaced by a mixture of xylene and paraffin (1:1) after two days at 45 °C. The sample tissue was permeated by pure paraffin after 4 days at 60 °C. After embedding, the samples were serially sectioned with a slicer Leica RM2145 (Leica, U.S.A), at a slice thickness of 4–5 μm. After the sections were deparaffinized, they were stained with 0.5% toluidine blue and transparent with xylene. After sealing the sections with neutral resin, they were observed with a Leica DM4 B microscope (Leica, U.S.A).

RNA extraction and RNA-Seq

Three representative stages 15 DAP (S1), 20 DAP (S2), and 25 DAP (S3) of female inflorescence were collected, frozen in liquid nitrogen, and stored at -80 °C. Total RNA was extracted using the CTAB method [46]. The cDNA library was constructed using the MGIEasy Fast PCR-Free Enzymatic Library Preparation Kit (MGI, China). The RNA quality was checked using Agilent 2100 Bioanalyzer (Agilent Technologies, CA, USA), and the raw sequences were obtained by sequencing using DNBSEQ-T7.

Differentially expressed genes identification

Filtration of low-quality reads was carried out to generate clean reads by using fastp [47]. The trimmed reads were then aligned to the *Betula platyphylla* v1.1 reference genome by STAR (v2.7.11b) [48, 49]. RNA-Seq by RSEM (v1.3.3) was used to quantify transcripts and the results were merged using the Transcripts per million (TPM) normalization method [50]. For genes with row means of TPM greater than one across the three stages of female inflorescence development, PCA analyses were performed using Log_2 (TPM + 1) values, then plotted with prcomp function in R. The DESeq2 (R package, v1.42.1) was used to identify the differentially expressed genes (DEGs) with thresholds of adjusted p-value < 0.05, and the absolute log_2 fold change ($|log_2FC|$) > 1 [51]. The resulting DEGs were annotated and transcription factor families were counted using the PlantTFDB database (https://planttfdb.gao-lab.org/aboutus.php) [52].

Gene co-expression network analysis

Weighted Gene Co-expression Network Analysis (WGCNA, R package) was used to generate the gene network following a step-by-step approach [53]. Data were obtained from three birch samples (four leaf samples, three pollen samples, and nine female inflorescence samples) [54, 55]. The median absolute deviation (MAD) of the expression of each gene was calculated to screen for genes with MAD > 0.01. Genes with a median absolute deviation (MAD) of gene expression greater than 0.01 were hierarchically clustered using the hclust function in R. The "network type" is selected as "signed" when "R^2" is greater than 0.85 to filter the soft threshold power. The step-by-step method calculates the adjacency matrix, then converts it to the topological overlap matrix, and finally to the distance matrix for module partitioning with the following arguments: "deepSplit" = 2, "MEDissThres" = 0.25, "minClusterSize" = 50. Hubgenes were filtered based on the threshold where the absolute value of module membership ($|MM|$) > 0.8 and the absolute

value of gene significance (|GS|) > 0.2. The hub gene sets obtained above were annotated to assign them to functional Gene Ontology (GO) categories by TBtools v.2.081 [56].

The quantitative real-time PCR analysis

The Synthesis SuperMix (TransGen, Beijing, China) was used for cDNA preparation. The TransStart® Top Green qPCR SuperMix (TransGen, Beijing, China) and a LightCycler480 system (Roche, Basel, Switzerland) were used to carry out the quantitative real-time PCR (RT-qPCR) program according to the instructions of the manufacturer. Based on the stability value of gene expression, the best reference gene is screened out by NormFinder (R package) [57]. The data was analyzed using the $2^{-\Delta\Delta Ct}$ method with *BpUBC32* (*BPChr08G07651*) as the internal control [58]. The experiment was carried out using three biological and technical replicates. The primers used for RT-qPCR are listed in Table S1.

Quantification of cell wall components

Cell wall composition was quantitatively analyzed across three developmental stages of birch female inflorescences (S1, S2, S3) using commercial assay kits: lignin content (G0708W), cellulose content (G0715W), hemicellulose content (G0716W), total pectin content (G0717W), and pectin methylesterification degree (G0723W) (Grayscale Biotechnology Co., Ltd., Suzhou, China). Three biological replicates per stage were analyzed, each with two technical replicates, following standardized protocols provided by the manufacturer.

Results

Development of female gametophyte and fertilization in Birch occurs after pollination

To ensure an accurate collection of female inflorescences at different developmental stages, a paraffin thin section was used to systematically define FG development and post-pollination stages in birch (Fig. 1 and Table S2).

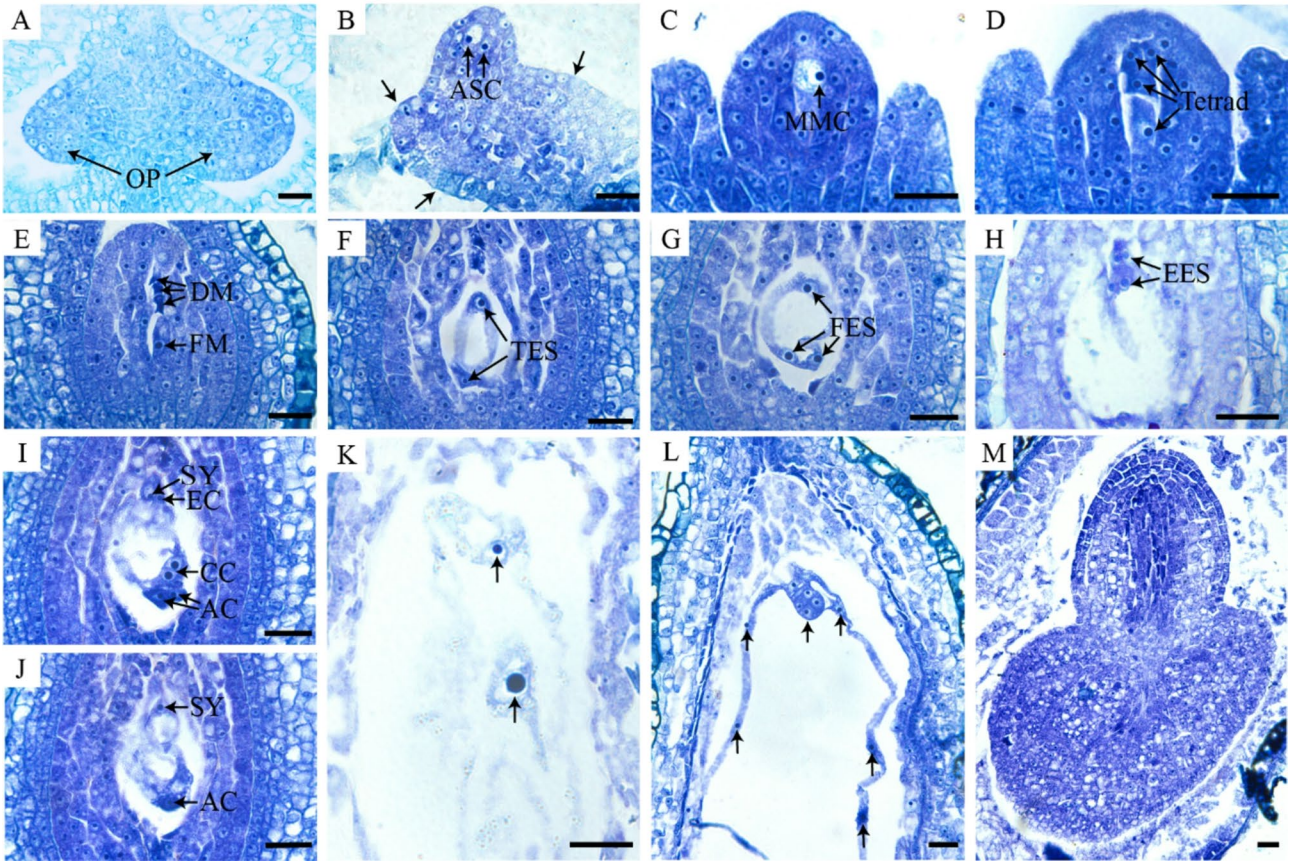

Fig. 1 Female gametophyte development of birch. (**A**) Ovule primordium. (**B**) Ovule at the stage of an ASC with integument primordium. (**C**) Nucellus at the stage of MMC. (**D**) Four megaspores and integuments. (**E**) Nucellus at the stage of functional megaspore. (**F**) Nucellus at the stage of TES. (**G**) Nucellus at the stage of FES. (**H**) Nucellus at the stage of EES. (**I**) Nucellus at the stage of MES. (**J**) Nucellus at the stage of MES (A continuous slice of the previous one). (**K**) Nucellus at the stage of fertilization. (**L**) The proembryo. (**M**) Embryo at a late stage of development. ASC, archesporial cell; MMC, megaspore mother cell; DM, degenerative megaspore; FM, functional megaspore; TES, two-nuclei embryo sac; FES, four-nuclei embryo sac; EES, eight-nuclei embryo sac; SY, synergid cell; EC, egg cell; CC, central cell; AC, antipodal cell. Scale bars = 20 μm

After pollination, female inflorescence increases in longitudinal and transverse diameter (Fig. S1 and S2). Female inflorescences at 0–9 DAP were found to be in the ovule primordium stage, with one ovule per locule. The ASCs form within the nucellus at 10–12 DAP, and most of the ovules have a single ASC, and a few have two ASCs (Fig. 1A and B). FGs develop to the MMC stage, with the ASC elongating and differentiating into the MMC, and a single integument covering half of the nucellus at 13–16 DAP (Fig. 1C). The MMC undergoes two meiotic divisions and forms four megaspores, three of which degenerate and only one FM at the chalazal end remains, and the micropyle forms at 17–20 DAP (Fig. 1D and E). At 21–25 DAP, three consecutive mitotic divisions occur to form a two-nuclei embryo sac (Fig. 1F), four-nuclei embryo sac (Fig. 1G), and eight-nuclei embryo sac (Fig. 1H). These eight nuclei undergo nuclear migration and cellularization to form an MES (Fig. 1I and J), one egg cell (EC), two synergids (SYs), one central cell (CC), including two polar nuclei, and three antipodal cells (ACs). Finally, the MES undergoes double fertilization (Fig. 1K), and embryos develop and mature (Fig. 1L and M).

Generation and analysis of transcriptome data from three developmental stages of Birch female inflorescence

RNA-seq analysis was performed on birch female inflorescences collected from three distinct developmental stages: the MMC stage (S1), the FM stage (S2), and the MES stage (S3). A total of approximately 464 million high-quality clean reads were generated. The generated clean reads were aligned to the *B. platyphylla* reference genome, with 95% alignment for each sample, of which more than 85% were uniquely identified (Table S3). The clean reads were processed and utilized for initial transcriptome analysis, resulting in the generation of gene expression matrices. Principal component analysis (PCA) was performed on the transcriptome data (Fig. 2A), and the results showed clear separation of samples at different developmental stages and proximity of samples within groups. PC1 (38.61%) and PC2 (14.97%) accounted for 53.58% of the total variance of the data, which had a high degree of explanatory power. The PCA results indicated that our transcriptome data had obvious clustering characteristics and good intergroup reproducibility, and could be used for further analysis. Using DESeq2 to identify DEGs at different developmental stages, volcano plots showed that S2 vs. S3 had far more DEGs than S1 vs. S2 and a greater average number of differential multiplicities

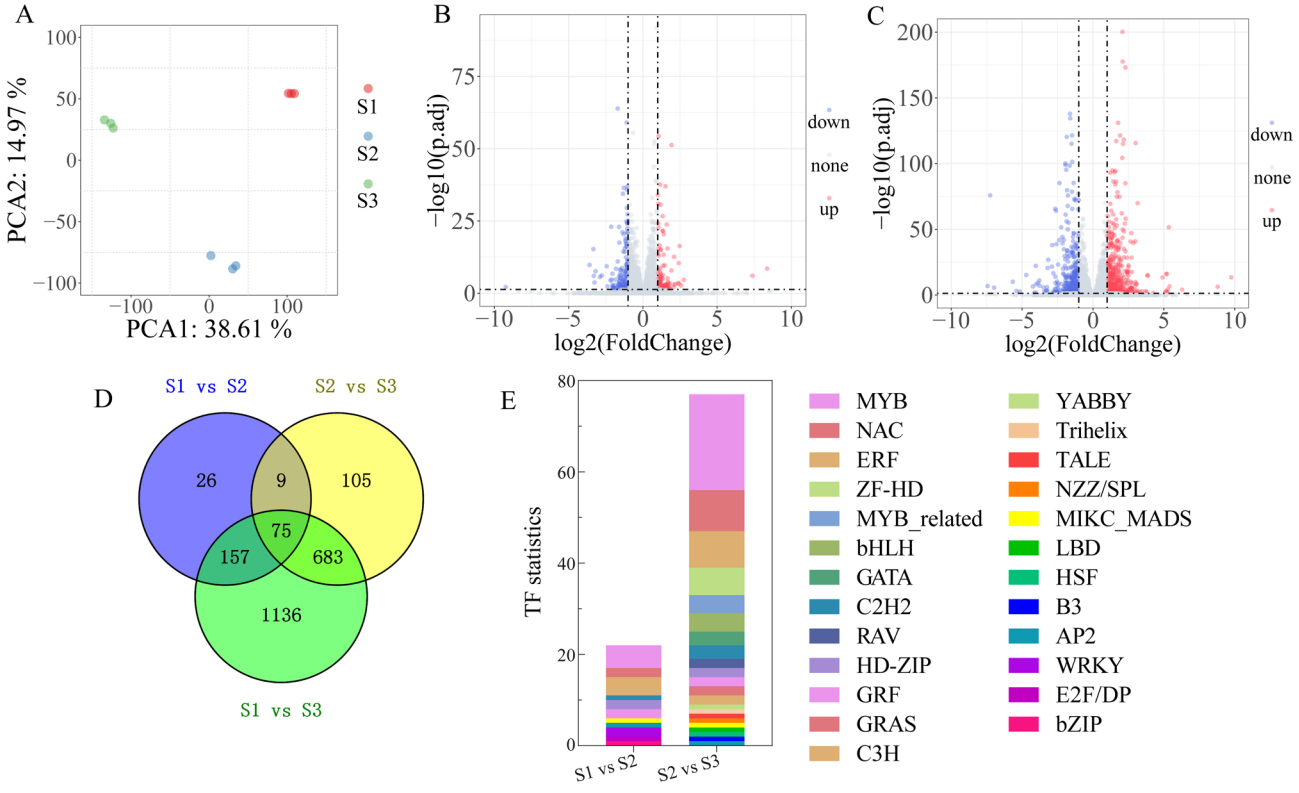

Fig. 2 Summary of RNA-seq data for 9 RNA samples from birch female inflorescence. (**A**) PCA plot. (**B**) Volcano plot of the transcriptome between S1 vs. S2. (**C**) Volcano plot of the transcriptome between S2 vs. S3. (**D**) Venn diagrams between S1 vs. S2, S2 vs. S3, and S1 vs. S3. (**E**) Transcription factors are differentially expressed in three periods

(Fig. 2B and C), suggesting that more genes are differentially expressed in the development of FMs to MESs than in the development of MMCs to FMs. This was confirmed by the Venn plots, which screened 267 DEGs for S1 vs. S2 and 872 DEGs for S2 vs. S3, with 84 common DEGs for the two comparative groups, and 75 common DEGs for all three comparative groups (Fig. 2D). The composition of transcription factor families in DEGs from S1 vs. S2 and S2 vs. S3 were counted and found MYB, NAC, and ERF TFs family were the most abundant in all the groups (Fig. 2E).

Co-expression network analyses reveal specific ROS and cell wall genes related to birch female inflorescence development.

The inflorescence transcriptomes were combined with four leaf transcriptomes and three staminate catkins transcriptomes, and a sample dendrogram was drawn to examine the clustering of the samples (Fig. 3A). WGCNA was constructed to identify key genes for female inflorescence development based on the correlation with the three female inflorescence developmental stages, and a dendrogram of gene clusters delineating modules and similar modules merged was plotted. As a result, a total of nine co-expression modules were identified of which the "antiquewhite4" module was significantly and positively correlated with the trait S1 (PCC > 0.7, $p < 0.05$), and the "plum2" module with the trait S3 positively correlated (PCC = 0.95, $p = 3.0 \times 10^{-08}$) based on the Pearson correlation coefficient (PCC) (Fig. 3B and C).

Then, MM and GS were combined to identify Hubgenes of the above two modules and performed GO enrichment analysis separately. The Hubgenes were listed in Table S4 and Table S5. For S1, a total of 95 clustered genes were screened, and GO enrichment analysis showed significant enrichment for lipid anabolism and regulation of hormone levels (Fig. 3D). A total of 100

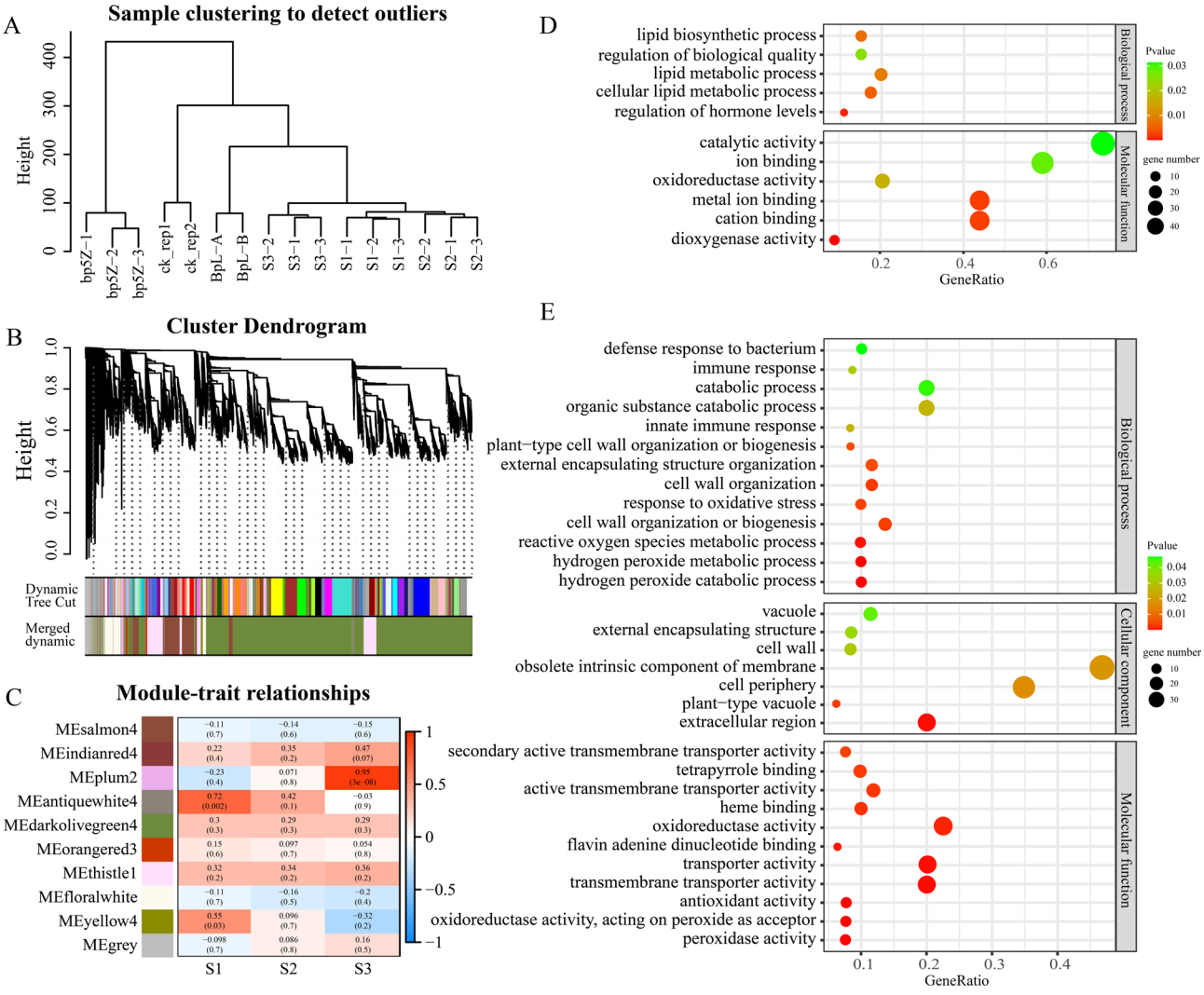

Fig. 3 Weighted gene co-expression network analysis. (**A**) Transcriptomes sample clustering. (**B**) Cluster dendrogram. (**C**) Module-trait relationships. (**D**) GO enrichment analysis of the antiquewhite4 module. (**E**) GO enrichment analysis of the plum2 module

clustered genes were screened by S3, which was significantly enriched in oxidoreductase activity and cell wall organization or biogenesis (Fig. 3E). These included genes annotated as peroxidases, which catalyze the degradation of H_2O_2, all of which were specifically overexpressed in S3 samples. Expression of genes involved in ROS regulation, *BpMKK3*, *BpMRP4*, and *BpGRX* progressively increased from S1 to S3. The obtained cell wall-related genes *BpPER25*, *BpPER66*, *BpMUCI21*, *BpXTH23*, *BpPME15*, *BpPGLR4*, *BpHHT1*, *BpMYB52*, *BpNAC25*, and *BpMYB26*, involved in cell wall generation, degradation, and modification were all highly expressed at S3.

Expression profiling reveals stage-specific ROS genes related to Birch female inflorescence development

We extensively characterized the transcript expression level of ROS-related genes and identified their specific expression patterns at different stages of female inflorescence development in birch (Fig. 4A-C). At S1, we observed high expression of *BpGSTU17* and *BpAPX1* throughout megasporogenesis, while *BpPRXIIE-1*, *BpSODCP*, *BpFDX3*, and *BpGSTU19* exhibited high expression levels in early megasporogenesis suggesting their role in early megasporogenesis. Notably, *BpPAO2* exhibited significantly high expression exclusively during the S2, indicating its potential role as a key regulator in FM formation.

Moreover, at S3, key genes involved in ROS homeostasis, including *BpACX*, *BpCuAOγ1*, *BpGLO1*, *BpRBOHH*, *BpUOX2*, *BpFSD2*, *BpCAT3*, *BpGRX*, *BpNRX*, and *BpTRX*, displayed significantly heightened expression levels. This suggests that both ROS synthesis and scavenging pathways are highly active at S3, potentially facilitating normal embryo sac development.

The genes related to cell wall biosynthesis were notably elevated during the mature embryo sac stage.

The cell wall-related genes including lignin, cellulose, hemicellulose and pectin biosynthesis were identified and found to be differentially expressed during the birch female inflorescence development (Fig. 5A-E). Cell wall biosynthesis is an important process encompassing a large number of proteins and regulatory factors, however, most cell wall synthesis-related genes were specific to the S3 stage. For the lignin biosynthesis pathway,

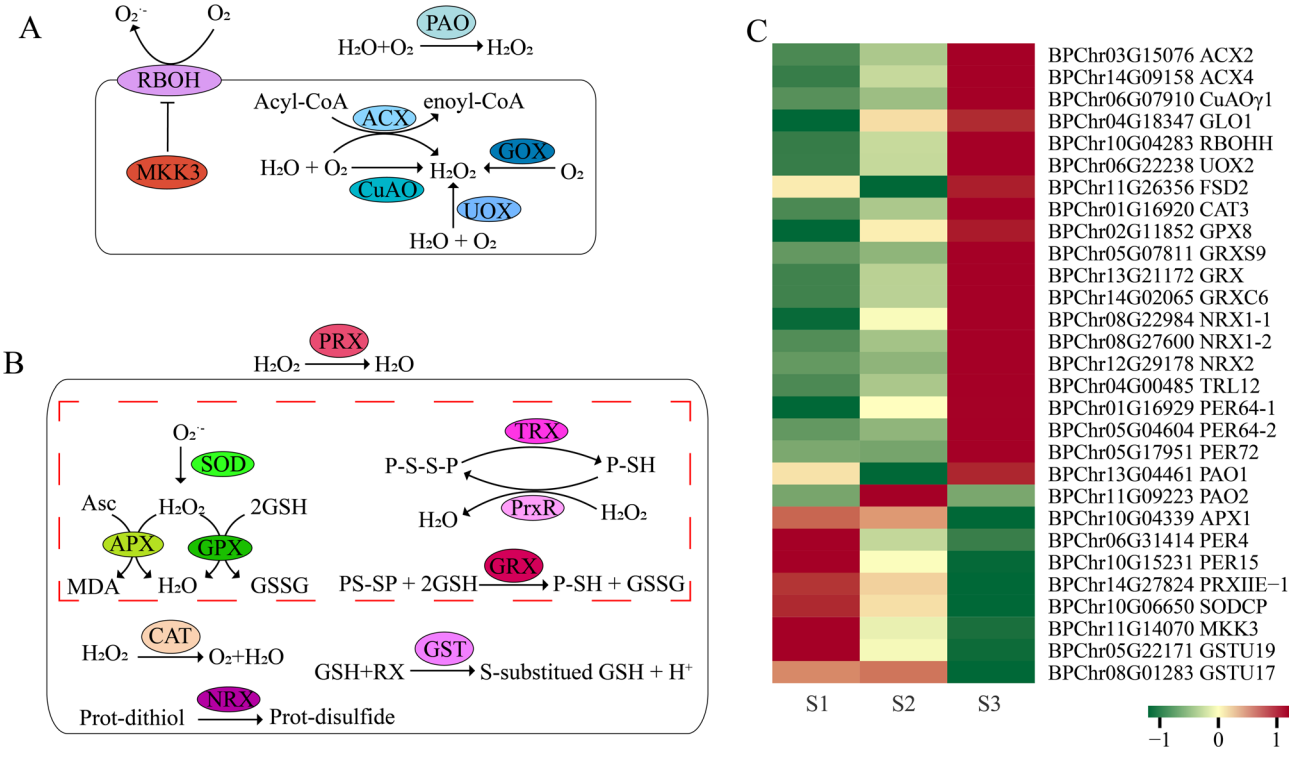

Fig. 4 Expression profile of ROS biosynthesis and scavenging related genes. (**A**) ROS synthesis-related pathway. (**B**) ROS scavenging-related pathways. (**C**) Heatmap of DEGs in ROS synthesis and scavenging-related pathways. The colors represent different expression levels. ACX, acyl-CoA oxidase; APX, ascorbate peroxidase; CAT, catalase; CuAOγ1, copper amine oxidases gamma 1; FSD2, superoxide dismutase [Fe] 2, chloroplastic; GLO1, glycolate oxidase 1; GOX, glycolate oxidase; GPX, glutathione peroxidase; GRX, glutaredoxin; GRXC6, glutaredoxin-C6; GRXS9, monothiol glutaredoxin-S9; GST, glutathione S-transferase; GSTU17, glutathione S-transferase U17; GSTU19, glutathione S-transferase U19; MKK3, mitogen-activated protein kinase kinase 3; NRX, nucleoredoxin; PAO, polyamine oxidase; PER, peroxidase; PrxR, peroxiredoxin; PRXIIE-1, peroxiredoxin-2E-1; RBOH, respiratory burst oxidase homologs; RBOHH, respiratory burst oxidase homolog protein H; SODCP, superoxide dismutase [Cu-Zn], chloroplastic; TRX, thioredoxin family; TRL12, TRX-LIKE 12; UOX, urate oxidase

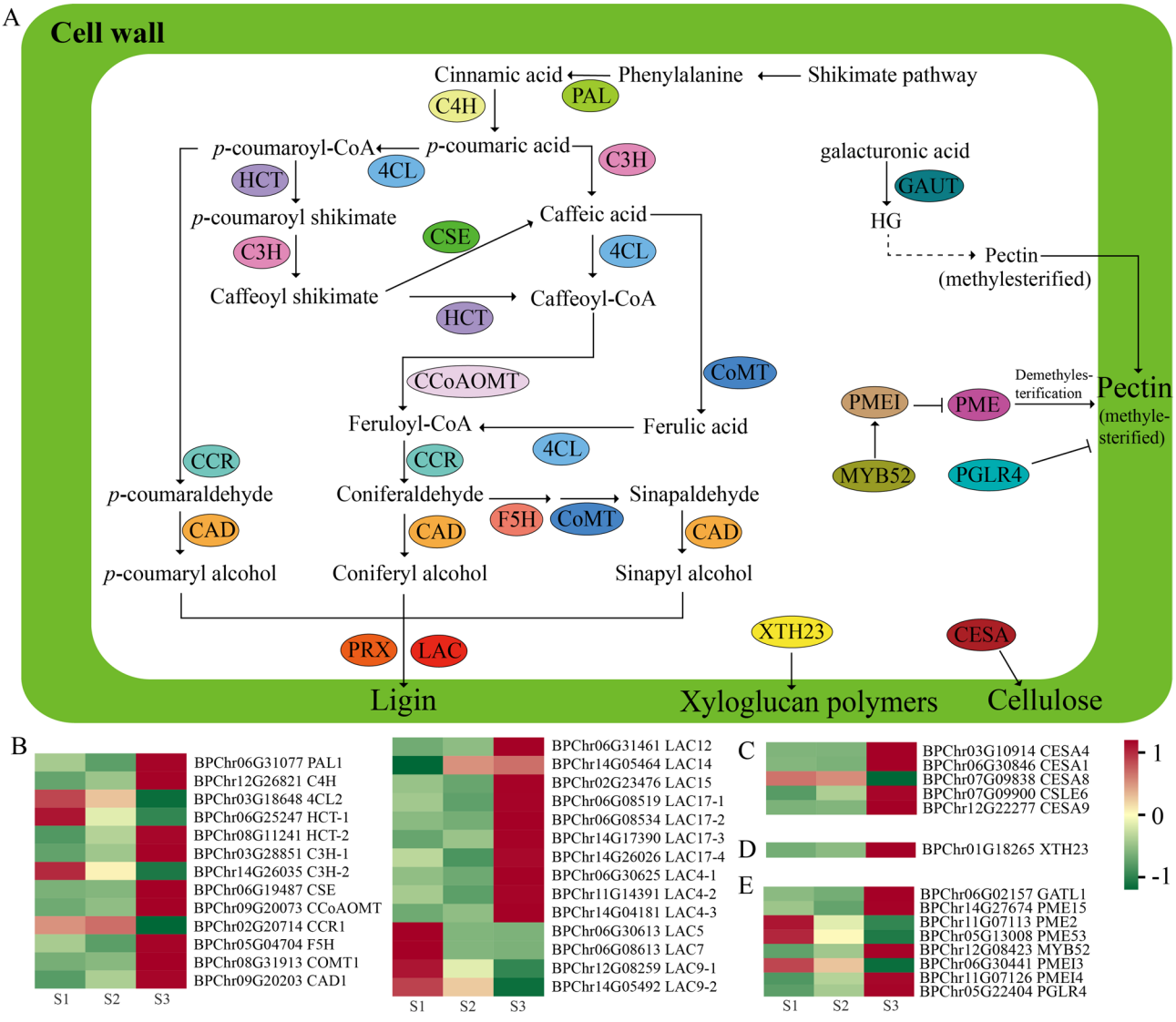

Fig. 5 Expression levels of genes related to the cell wall biosynthesis pathway. (**A**) Cell wall biosynthesis-related pathways. (**B**) DEGs in lignin biosynthesis-related pathways. (**C**) DEGs in cellulose biosynthesis-related pathways. (**D**) DEGs in hemicellulose biosynthesis-related pathways. (**E**) DEGs in pectin biosynthesis-related pathways. The color scale indicates normalized expression levels. PAL, phenylalanine ammonia-lyase; C4H, cinnamate 4-hydroxylase; 4CL, 4-coumarate CoA ligase; CCR, cinnamoyl-CoA reductase; HCT, hydroxycinnamoyl-CoA shikimate/Quinatehydroxycinnamoyltransferase; C3H, *p*-coumarate 3-hydroxylase; CCoAOMT, caffeoyl-CoA *O*-methyltransferase; F5H, ferulate 5-hydroxylase; CSE, caffeoyl shikimate esterase; COMT, caffeic acid O-methyltransferase; CAD, cinnamyl alcohol dehydrogenase; LAC, laccase; PRX, peroxiredoxin; CESA, cellulose synthase A; CSLE6, cellulose synthase-like protein E6; XTH23, xyloglucan endotransglucosylase/hydrolase 23; GAUT, galacturonosyltransferase; GATL1, GAUT-like 1; PME, pectin methylesterases; PMEI, pectin methylesterase inhibitor; PGLR4, polygalacturonase 4

phenylalanine ammonia-lyase (PAL) and cinnamate 4-hydroxylase (C4H), which are the key enzymes, are both highly expressed in S3; caffeoyl shikimate esterase (CSE), caffeic acid O-methyltransferase (CoMT), caffeoyl-CoA *O*-methyltransferase (CCoAOMT), cinnamyl alcohol dehydrogenase (CAD), ferulate 5-hydroxylase (F5H), and laccase (LAC) are highly expressed in S3, whereas 4-coumarate CoA ligase (4CL) and cinnamoyl-CoA reductase (CCR) have high expression in S1 and S2. Meanwhile, *BpHCT-1* and *BpC3H-2* were highly expressed in S1, but *BpHCT-2* and *BpC3H-1* were highly expressed in S3. The synthesis of cellulose and xyloglucan (the main hemicellulose) is mediated by cellulose synthase A (CESA) and xyloglucan endotransglucosylase/hydrolase 23 (XTH23), respectively, with both genes exhibiting high expression levels during the S3. For the pectin biosynthesis pathway, GAUT synthesizes HG, a precursor substance of pectin was found to be highly expressed at S3. However, repressors such as *BpMYB52* and *BpPMEI4* were highly expressed at S3. Meanwhile, *BpPME2* and *BpPME53* were expressed highly during the

S1 stage, while *BpPME15* was expressed highly during the S3 stage.

The quantitative real-time PCR validation of candidate genes

Several genes were subjected to RT-qPCR analyses for RNA-seq data validation. The *BpACX2*, *BpCAT3*, *BpTRL12*, *BpPER64*-1, and *BpRBOHH* showed a gradual increase in expression level throughout the S1, S2, and S3 stages, while *BpSODCP* showed a gradual decrease in expression level from S1 to S3, and *BpPAO2* showed higher expression level in S2 stage only (Fig. 6A). For the cell wall-related genes, two genes related to lignin biosynthesis, *BpPAL1* and *BpLAC12*, and one gene related to cellulose biosynthesis *BpCESA4* showed higher expression level in S3. One hemicellulose biosynthesis-related gene, *BpXTH23*, showed higher expression in the S3. Moreover, three pectin biosynthesis-related genes, *BpGATL1*, *BpPGLR4*, and *BpMYB52*, showed higher expression in S3, while *BpPME53*, which is related to pectin biosynthesis, showed a gradual decrease from S1 to S3 (Fig. 6B). The data and revealed that the selected genes play a major role in the maturation of embryo sac.

Temporal regulation of cell wall components during Birch female inflorescence development

The dynamic changes in lignin, cellulose, hemicellulose, and pectin content, along with pectin methylesterification degree (PMD) were quantified across three developmental stages (S1, S2, S3) of birch female inflorescences. Lignin content showed a significant increase at S3 compared to S1 and S2, with no statistically significant difference observed between S1 and S2. Cellulose and hemicellulose contents exhibited a progressive accumulation from S1 to S3. Conversely, total pectin content decreased markedly during this developmental progression, while PMD exhibited an increasing trend. These results highlight the critical role of stage-specific cell wall remodeling during embryo sac maturation in birch female inflorescence development (Fig. 7).

Discussion

The female gametophyte development in birch plants consists of the formation of the FM from the MMC, and the formation of a structurally complex seven-cell embryo sac from the FM [3, 59]. These processes are crucial for the development of FG in plants and are well studied [60, 61]. After pollination, the female inflorescence enlarges and increases in diameter longitudinaly and transversely followed by FG maturation at S3 (Fig. S1). There is a long interval between pollination and fertilization in birch [62]. All developmental stages and corresponding cellular structures of birch female inflorescences from stigma maturation to double fertilization were identified from the histological perspective (Fig. 1). Consequently, the birch flower is flocculus in nature, whose complex structure and tiny female flowers impede the observation of developmental processes. As a result, studies of FG development in birch are still at a very preliminary stage.

Transcriptomic technology is important in exploring the intricacies of plant reproduction. Many studies used transcriptomics to explore the development of plants male and female flowers [63–65]. Here, 464 million high-quality clean reads were generated from three developmental stages, MMC, FM, and MES. A total of 2,191 genes were expressed differentially, and PCA showed clear differentiation of samples at different developmental stages, indicating that all the genes are differentially expressed in all groups. The composition of transcription factor families in the DEGs showed that families of MYB, NAC, and ERF TFs were the most abundant in all the groups (Fig. 2). Many studies suggest how weighted gene co-expression network analysis is employed to establish a gene functional relationship [66, 67]. Here, our data revealed key genes involved in specific female inflorescence development stages (Table S4 and S5), these genes regulate oxidoreductase activity and cell wall organization or biogenesis during flower development (Fig. 3E).

Our study revealed that the expression of *BpMKK3* and its expression progressively increased from S1 to S3. In *Arabidopsis MKK3* and *MKK4* were found to regulate ROS and H_2O_2 via the MAPK pathway [68]. *MKK3* is involved in negative regulation ROS accumulation through the MAP kinase phosphorylation cascade in *Arabidopsis* [69]. Expression of *BpMRP4* and *BpGRX* progressively increased from S1 to S3, these genes are involved in the transport of GSH and oxidized glutathione (GSSG) and are both associated with antioxidants. (Figure 4A and B). Many studies suggest that ROS homeostasis is a key form of ROS action in influencing female inflorescence development, particularly mitochondrial ROS [5]. However, our results indicate that many non-mitochondrial ROS show significant specificity in their expression, suggesting that these ROS are important in regulating different stages of female inflorescence development. We observed that only the genes for scavenging ROS were highly expressed in the MMC stage, which is consistent with the idea that ROS levels are generally maintained at a low level in plant systems [70]. In contrast, at the S2 stage, the transcript level of the genes that scavenge ROS was greatly reduced, while the gene that generates ROS, *BpPAO2*, was highly expressed. This unique expression pattern shows that it may be playing a role in the specific regulation of FM development. Moreover, genes that produce ROS such as RBOH as well as genes that scavenge ROS, are highly expressed in the MES stage. This may imply that ROS signaling is

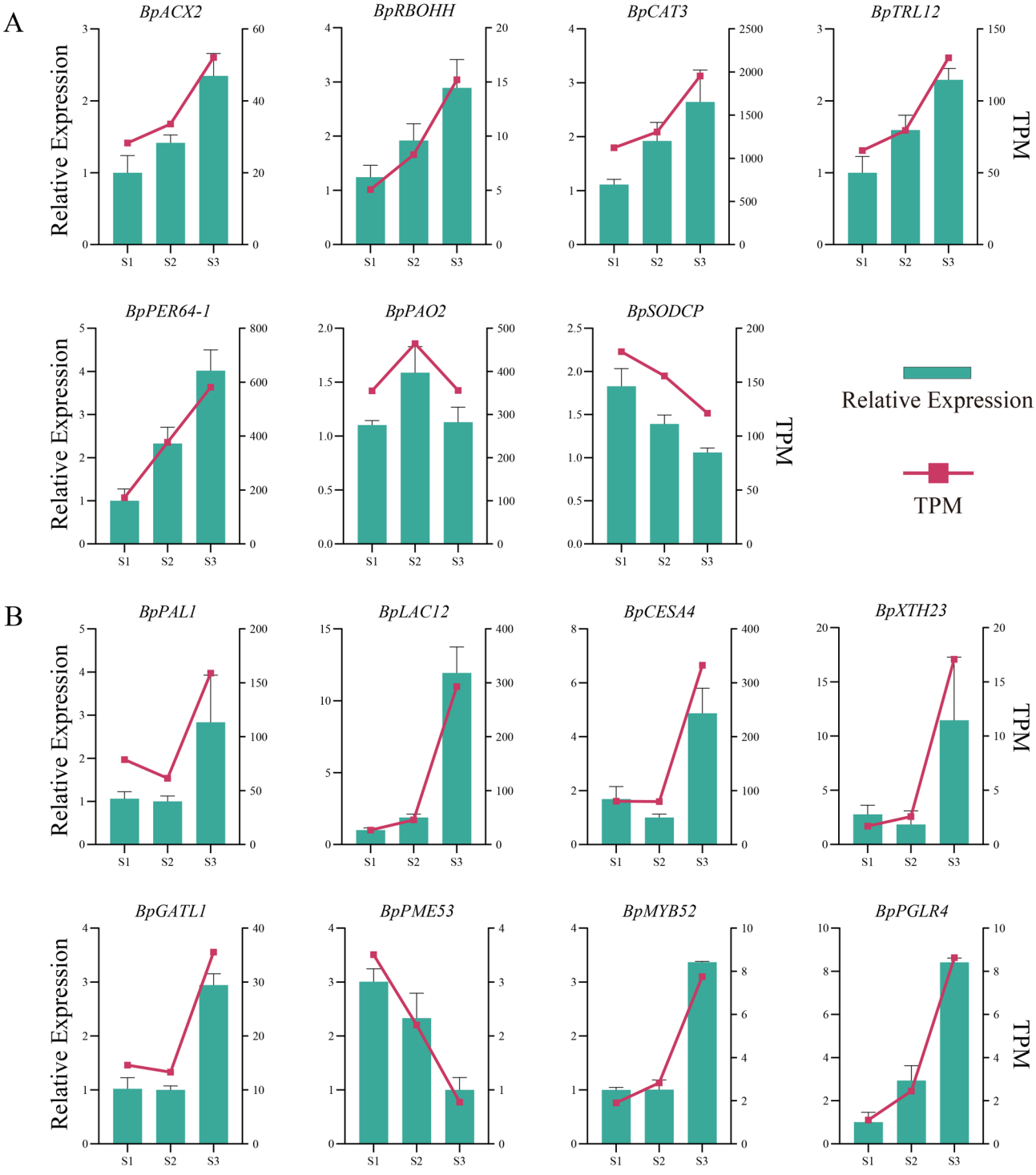

Fig. 6 The expression verification of candidate genes by RT-qPCR. (**A**) ROS synthesis and scavenging-related genes. (**B**) Cell wall biosynthesis related genes. The selected gene expression levels derived by the TPM normalization method are shown on the right Y-axis, while the relative gene expression levels determined by RT-qPCR are shown on the left Y-axis. Data are presented as means and ± SE of three biological replicates

generated and used to regulate the development of the MES. At the same time, genes that scavenge ROS are highly activated to regulate ROS homeostasis and prevent oxidative damage (Fig. 4C).

Cell wall biosynthesis, degradation, and modification-related genes were predominantly upregulated during the S3 stage (Fig. 5A-E). Elevated expression of lignin biosynthesis genes such as *BpLAC* indicated active lignification.

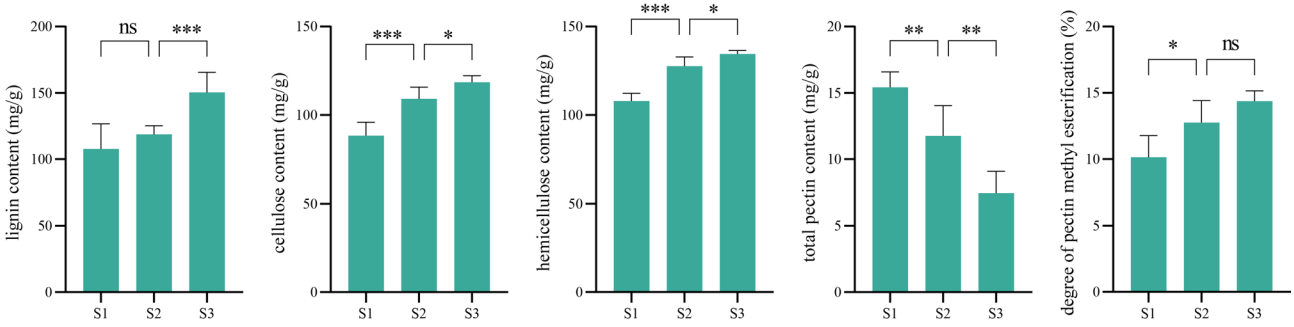

Fig. 7 Changes in the contents of lignin, cellulose, hemicellulose, pectin and pectin methylesterification degree during the development of birch female inflorescences at stages S1, S2, and S3. All data are from three biological replicates and are expressed as means ± SD (ns, not significant; *, $p < 0.05$; **, $p < 0.01$; ***, $p < 0.001$; one-way analysis of variance (ANOVA))

BpPER25 and *PER66*, involved in lignin biosynthesis and degradation [71], along with *HHT1* (contributing to suberin aromatic polymer synthesis) [72], showed peak expression in S3 (Table S5). Previous studies demonstrated that controlled lignin deposition during megaspore development (S1 and S2 stages) reduces cell wall tension to restrict cellular overexpansion, thereby regulating ovule size [73–75], a mechanism consistent with the observed lignin accumulation in S3 (Fig. 7). Notably, *BpHCT-1*, *BpC3H-2*, and *BpCCR1* were upregulated during S1, as were key downstream enzyme genes (*BpLAC7*, *BpLAC9-1*, and *BpLAC9-2*), suggesting their roles in synthesizing phenylpropanoid derivatives. During S3, coordinated high expression of enzymatic genes, including *BpCESAs* and *BpXTH23* contributing substantial cellulose and hemicellulose production (Figs. 5C-D and 7). This biosynthetic phase coincided with intensive nucellar cell division and structural remodeling, leading to a marked increase in nucellar cell layers. The combinatorial synthesis of rigid cellulose microfibrils and flexible matrix polysaccharides likely modulates cell wall extensibility at this developmental stage [73, 76]. Cell wall composition analysis revealed decreased pectin content during S3 despite active synthesis of other structural components. Pectin-mediated developmental regulation occurs through methylation dynamics [41]. Upregulated *BpGAUT* enhanced pectin synthesis, while *BpMYB52* suppressed pectin demethylation by repressing PME activity. Concurrently, *BpPGLR4*-mediated degradation of demethylated pectin refined cell wall architecture (Fig. 7). The predominant deposition of methyl-esterified pectin, coupled with lignin accumulation, enhanced mechanical strength to stabilize the mature female inflorescence structure, establishing the foundation for subsequent fertilization [77].

Conclusions

In the current study, the histological thin sections results showed that the MMC stage, FM stage, and MES stage were the critical stages in birch female inflorescence development. Our study through transcriptome analyses revealed regulatory factors during the birch female inflorescence development. We showed that ROS homeostasis favors the process of birch megasporogenesis, while ROS signaling may participate in the development of the embryo sac. In addition, cell wall synthesis related genes participate in the maturation process of the embryo sac. These findings provide useful information for further understanding of birch reproductive development.

Supplementary Information

The online version contains supplementary material available at https://doi.org/10.1186/s12870-025-06740-2.

Supplementary Material 1: Supplementary figure S1: External morphology of birch female inflorescence. (A-P) Female inflorescence of 0, 5, 10, 15, 18, 20, 22, 24, 25, 27, 30, 33, 36, 40, 45 and 50 days after pollination. Scale bars = 1 cm. Supplementary figure S2: Changes in the longitudinal and transverse diameter of birch female gametophyte development. The values represent the mean ± the standard deviation ($n = 10$). Different letters indicate significant differences between the means ($P < 0.05$). Significant differences in longitudinal diameter are marked with lowercase letters above the line, and differences in transverse diameter are marked with capital letters above the line.

Supplementary Material 2: Supplementary Table S1: Primers for RT-qPCR. Supplementary Table S2: Definition of the stages of birch female gametophyte development. Supplementary Table S3: Transcriptome sequencing statistics and quality evaluation of birch female inflorescence. Supplementary Table S4: WGCNA results for hubgene in the "antiquewhite4" module. Supplementary Table S5: WGCNA results for hubgene in the "plum2" module.

Author contributions

X.G.L. and J.J. had the idea for and designed the study. X.G.L. management and coordination responsibility for the research activity planning and execution. K.H.Z. did the statistical analysis. M.J.C, K.H.Z, B.H.J, L.L.L, J.Y.S, X.Z, P.W, and H.N.Z drafted the manuscript. X.G.L. and B.H.J. provided critical editing of the manuscript. All authors read and approved of its content.

Funding

This research was supported by the National Key R&D Program of China during the 14th Five-year Plan Period (2021YFD2200105), and the Heilongjiang Touyan Innovation Team Program (Tree Genetics and Breeding Innovation Team).

Data availability

No datasets were generated or analysed during the current study.

Declarations

Ethics approval and consent to participate
Not applicable.

Consent for publication
Not applicable.

Competing interests
The authors declare no competing interests.

Received: 5 May 2024 / Accepted: 19 May 2025
Published online: 27 May 2025

References

1. Drews GN, Koltunow AM. The female gametophyte. Arabidopsis Book. 2011;9:e0155.
2. Mao B, Zheng W, Huang Z, Peng Y, Shao Y, Liu C, et al. Rice MutLγ, the MLH1-MLH3 heterodimer, participates in the formation of type I crossovers and regulation of embryo sac fertility. Plant Biotechnol J. 2021;19:1443–55.
3. Yang WC, Shi DQ, Chen YH. Female gametophyte development in flowering plants. Annu Rev Plant Biol. 2010;61:89–108.
4. Shi DQ, Yang WC. Ovule development in arabidopsis: progress and challenge. Curr Opin Plant Biol. 2011;14:74–80.
5. Ali MF, Muday GK. Reactive oxygen species are signaling molecules that modulate plant reproduction. Plant Cell Environ. 2024;47:1592–605.
6. Qin H, Li H, Abhinandan K, Xun B, Yao K, Shi J, et al. Fatty acid biosynthesis pathways are downregulated during stigma development and are critical during Self-Incompatible responses in ornamental Kale. Int J Mol Sci. 2022;23:13102.
7. Wang M, Tian D, Li T, Pan J, Wang C, Wu L, et al. Comprehensive identification and functional characterization of GhpPLA gene family in reproductive organ development. BMC Plant Biol. 2023;23:599.
8. Rhee SG. Cell signaling. H_2O_2, a necessary evil for cell signaling. Science. 2006;312:1882–3.
9. D'Autréaux B, Toledano MB. ROS as signalling molecules: mechanisms that generate specificity in ROS homeostasis. Nat Rev Mol Cell Biol. 2007;8:813–24.
10. Considine MJ, Foyer CH. Redox regulation of plant development. Antioxid Redox Signal. 2014;21:1305–26.
11. Miao Y, Lv D, Wang P, Wang XC, Chen J, Miao C, et al. An Arabidopsis glutathione peroxidase functions as both a redox transducer and a scavenger in abscisic acid and drought stress responses. Plant Cell. 2006;18:2749–66.
12. Wang C, Liu R, Lim GH, de Lorenzo L, Yu K, Zhang K, et al. Pipecolic acid confers systemic immunity by regulating free radicals. Sci Adv. 2018;4:eaar4509.
13. Huang X, Chen S, Li W, Tang L, Zhang Y, Yang N, et al. ROS regulated reversible protein phase separation synchronizes plant flowering. Nat Chem Biol. 2021;17:549–57.
14. Lan X, Yang J, Abhinandan K, Nie Y, Li X, Li Y, et al. Flavonoids and ROS play opposing roles in mediating pollination in ornamental Kale (Brassica Oleracea Var. acephala). Mol Plant. 2017;10:1361–4.
15. Lennicke C, Cochemé HM. Redox metabolism: ROS as specific molecular regulators of cell signaling and function. Mol Cell. 2021;81:3691–707.
16. Cheung EC, Vousden KH. The role of ROS in tumour development and progression. Nat Rev Cancer. 2022;22:280–97.
17. Heller J, Tudzynski P. Reactive oxygen species in phytopathogenic fungi: signaling, development, and disease. Annu Rev Phytopathol. 2011;49:369–90.
18. Murphy MP, Holmgren A, Larsson NG, Halliwell B, Chang CJ, Kalyanaraman B, et al. Unraveling the biological roles of reactive oxygen species. Cell Metab. 2011;13:361–6.
19. Paulsen CE, Carroll KS. Cysteine-mediated redox signaling: chemistry, biology, and tools for discovery. Chem Rev. 2013;113:4633–79.
20. Martin MV, Fiol DF, Sundaresan V, Zabaleta EJ, Pagnussat GC. oiwa, a female gametophytic mutant impaired in a mitochondrial manganese-superoxide dismutase, reveals crucial roles for reactive oxygen species during embryo sac development and fertilization in Arabidopsis. Plant Cell. 2013;25:1573–91.
21. Sankaranarayanan S, Ju Y, Kessler SA. Reactive oxygen species as mediators of gametophyte development and double fertilization in flowering plants. Front Plant Sci. 2020;11:1199.
22. Mittler R. ROS are good. Trends Plant Sci. 2017;22:11–9.
23. Chapman JM, Muhlemann JK, Gayomba SR, Muday GK, RBOH-Dependent ROS. Synthesis and ROS scavenging by plant specialized metabolites to modulate plant development and stress responses. Chem Res Toxicol. 2019;32:370–96.
24. Marino D, Dunand C, Puppo A, Pauly N. A burst of plant NADPH oxidases. Trends Plant Sci. 2012;17:9–15.
25. Jiménez-Quesada MJ, Traverso J, Alché Jde D. NADPH Oxidase-Dependent superoxide production in plant reproductive tissues. Front Plant Sci. 2016;7:359.
26. Cai K, Liu H, Chen S, Liu Y, Zhao X, Chen S. Genome-wide identification and analysis of class III peroxidases in Betula pendula. BMC Genomics. 2021;22:314.
27. Holley AK, Bakthavatchalu V, Velez-Roman JM, St Clair DK. Manganese superoxide dismutase: guardian of the powerhouse. Int J Mol Sci. 2011;12:7114–62.
28. Badawi GH, Kawano N, Yamauchi Y, Shimada E, Sasaki R, Kubo A, et al. Overexpression of ascorbate peroxidase in tobacco chloroplasts enhances the tolerance to salt stress and water deficit. Physiol Plant. 2004;121:231–8.
29. Rodriguez Milla MA, Maurer A, Rodriguez Huete A, Gustafson JP. Glutathione peroxidase genes in Arabidopsis are ubiquitous and regulated by abiotic stresses through diverse signaling pathways. Plant J. 2003;36:602–15.
30. Bhatt I, Tripathi BN. Plant Peroxiredoxins: catalytic mechanisms, functional significance and future perspectives. Biotechnol Adv. 2011;29:850–9.
31. Chronopoulou E, Ataya FS, Pouliou F, Perperopoulou F, Georgakis N, Nianiou-Obeidat I, et al. Structure, evolution and functional roles of plant glutathione transferases. Cham: Springer International Publishing; 2017.
32. Takahashi F, Mizoguchi T, Yoshida R, Ichimura K, Shinozaki K. Calmodulin-dependent activation of MAP kinase for ROS homeostasis in Arabidopsis. Mol Cell. 2011;41:649–60.
33. Vaahtera L, Schulz J, Hamann T. Cell wall integrity maintenance during plant development and interaction with the environment. Nat Plants. 2019;5:924–32.
34. Vanholme R, De Meester B, Ralph J, Boerjan W. Lignin biosynthesis and its integration into metabolism. Curr Opin Biotechnol. 2019;56:230–9.
35. Höfte H, Voxeur A. Plant cell walls. Curr Biol. 2017;27:R865–70.
36. Ellis C, Karafyllidis I, Wasternack C, Turner JG. The Arabidopsis mutant cev1 links cell wall signaling to jasmonate and ethylene responses. Plant Cell. 2002;14:1557–66.
37. Turner SR, Somerville CR. Collapsed xylem phenotype of Arabidopsis identifies mutants deficient in cellulose deposition in the secondary cell wall. Plant Cell. 1997;9:689–701.
38. Taylor NG, Laurie S, Turner SR. Multiple cellulose synthase catalytic subunits are required for cellulose synthesis in Arabidopsis. Plant Cell. 2000;12:2529–40.
39. Pauly M, Keegstra K. Biosynthesis of the plant cell wall matrix polysaccharide Xyloglucan. Annu Rev Plant Biol. 2016;67:235–59.
40. De Caroli M, Manno E, Piro G, Lenucci MS. Ride to cell wall: Arabidopsis XTH11, XTH29 and XTH33 exhibit different secretion pathways and responses to heat and drought stress. Plant J. 2021;107:448–66.
41. Du J, Anderson CT, Xiao C. Dynamics of pectic homogalacturonan in cellular morphogenesis and adhesion, wall integrity sensing and plant development. Nat Plants. 2022;8:332–40.
42. Atmodjo MA, Sakuragi Y, Zhu X, Burrell AJ, Mohanty SS, Atwood JA 3, et al. Galacturonosyltransferase (GAUT)1 and GAUT7 are the core of a plant cell wall pectin biosynthetic homogalacturonan:galacturonosyltransferase complex. Proc Natl Acad Sci U S A. 2011;108:20225–30.
43. Peaucelle A, Braybrook SA, Le Guillou L, Bron E, Kuhlemeier C, Höfte H. Pectin-induced changes in cell wall mechanics underlie organ initiation in Arabidopsis. Curr Biol. 2011;21:1720–6.
44. Hocq L, Guinand S, Habrylo O, Voxeur A, Tabi W, Safran J, et al. The exogenous application of AtPGLR, an endo-polygalacturonase, triggers pollen tube burst and repair. Plant J. 2020;103:617–33.
45. Shi D, Ren A, Tang X, Qi G, Xu Z, Chai G, et al. MYB52 negatively regulates pectin demethylesterification in seed coat mucilage. Plant Physiol. 2018;176:2737–49.
46. Doyle J. DNA protocols for plants-CTAB total DNA isolation. Mol Techniques Taxonomy. 1991;57:283–93.
47. Chen S, Zhou Y, Chen Y, Gu J. Fastp: an ultra-fast all-in-one FASTQ preprocessor. Bioinformatics. 2018;34:i884–90.
48. Chen S, Wang Y, Yu L, Zheng T, Wang S, Yue Z, et al. Genome sequence and evolution of Betula platyphylla. Hortic Res. 2021;8:37.
49. Dobin A, Davis CA, Schlesinger F, Drenkow J, Zaleski C, Jha S, et al. STAR: ultrafast universal RNA-seq aligner. Bioinformatics. 2013;29:15–21.

50. Li B, Dewey CN. RSEM: accurate transcript quantification from RNA-Seq data with or without a reference genome. BMC Bioinformatics. 2011;12:323.
51. Love MI, Huber W, Anders S. Moderated Estimation of fold change and dispersion for RNA-seq data with DESeq2. Genome Biol. 2014;15:550.
52. Jin J, Tian F, Yang DC, Meng YQ, Kong L, Luo J, et al. PlantTFDB 4.0: toward a central hub for transcription factors and regulatory interactions in plants. Nucleic Acids Res. 2017;45:D1040–5.
53. Langfelder P, Horvath S. WGCNA: an R package for weighted correlation network analysis. BMC Bioinformatics. 2008;9:559.
54. Ritonga F, Chen S, Indriani F, Song R, Zhang X, Lan X, et al. Comparative RNA-Seq analysis of Betula platyphylla under low and high temperature stresses. Cerne. 2023;29:2023.
55. Zhang J, Shi J, Zeng K, Cai M, Lan X. Transcriptomic landscape of staminate Catkins development during overwintering process in Betula platyphylla. Front Plant Sci. 2023;14:1249122.
56. Chen C, Wu Y, Li J, Wang X, Zeng Z, Xu J, et al. TBtools-II: A one for all, all for one bioinformatics platform for biological big-data mining. Mol Plant. 2023;16:1733–42.
57. Andersen CL, Jensen JL, Ørntoft TF. Normalization of real-time quantitative reverse transcription-PCR data: a model-based variance Estimation approach to identify genes suited for normalization, applied to bladder and colon cancer data sets. Cancer Res. 2004;64:5245–50.
58. Livak KJ, Schmittgen TD. Analysis of relative gene expression data using real-time quantitative PCR and the 2(-Delta Delta C(T)) method. Methods. 2001;25:402–8.
59. Yadegari R, Drews GN. Female gametophyte development. Plant Cell. 2004;16:S133–41.
60. Ashapkin VV, Kutueva LI, Aleksandrushkina NI, Vanyushin BF. Epigenetic regulation of plant gametophyte development. Int J Mol Sci. 2019;20:3051.
61. Erbasol Serbes I, Palovaara J, Groß-Hardt R. Development and function of the flowering plant female gametophyte. Curr Top Dev Biol. 2019;131:401–34.
62. Xin Q, Hu X, Zhang Y, Li D, Xu B, Liu X. Expression pattern analysis of key genes related to anther development in a mutant of male-sterile Betula platyphylla Suk. Tree Genet Genomes. 2020;16:33.
63. Wang S, Yang S, Jakada BH, Qin H, Zhan Y, Lan X. Transcriptomics reveal the involvement of reactive oxygen species production and sequestration during stigma development and pollination in Fraxinus mandshurica. Forestry Res. 2024;4:e014.
64. Quiapim AC, Brito MS, Bernardes LAS, daSilva I, Malavazi I, DePaoli HC, et al. Analysis of the Nicotiana tabacum stigma/style transcriptome reveals gene expression differences between wet and dry stigma species. Plant Physiol. 2008;149:1211–30.
65. Hu J, Liu Y, Tang X, Rao H, Ren C, Chen J, et al. Transcriptome profiling of the flowering transition in saffron (Crocus sativus L). Sci Rep. 2020;10:9680.
66. Niu X, Zhang J, Zhang L, Hou Y, Pu S, Chu A, et al. Weighted gene Co-Expression network analysis identifies critical genes in the development of heart failure after acute myocardial infarction. Front Genet. 2019;10:1214.
67. Chutimanukul P, Saputro TB, Mahaprom P, Plaimas K, Comai L, Buaboocha T, et al. Combining genome and gene Co-expression network analyses for the identification of genes potentially regulating salt tolerance in rice. Front Plant Sci. 2021;12:704549.
68. Dóczi R, Brader G, Pettkó-Szandtner A, Rajh I, Djamei A, Pitzschke A, et al. The Arabidopsis mitogen-activated protein kinase kinase MKK3 is upstream of group C mitogen-activated protein kinases and participates in pathogen signaling. Plant Cell. 2007;19:3266–79.
69. Verma D, Jalmi SK, Bhagat PK, Verma N, Sinha AK. A bHLH transcription factor, MYC2, imparts salt intolerance by regulating proline biosynthesis in Arabidopsis. Febs J. 2020;287:2560–76.
70. Mittler R, Zandalinas SI, Fichman Y, Van Breusegem F. Reactive oxygen species signalling in plant stress responses. Nat Rev Mol Cell Biol. 2022;23:663–79.
71. Zhao Q, Nakashima J, Chen F, Yin Y, Fu C, Yun J, et al. Laccase is necessary and nonredundant with peroxidase for lignin polymerization during vascular development in Arabidopsis. Plant Cell. 2013;25:3976–87.
72. Molina I, Li-Beisson Y, Beisson F, Ohlrogge JB, Pollard M. Identification of an Arabidopsis feruloyl-coenzyme A transferase required for suberin synthesis. Plant Physiol. 2009;151:1317–28.
73. Tucker MR, Koltunow AM. Traffic monitors at the cell periphery: the role of cell walls during early female reproductive cell differentiation in plants. Curr Opin Plant Biol. 2014;17:137–45.
74. Gawecki R, Sala K, Kurczyńska EU, Świątek P, Płachno BJ. Immunodetection of some pectic, Arabinogalactan proteins and hemicellulose epitopes in the micropylar transmitting tissue of apomictic dandelions (Taraxacum, Asteraceae, Lactuceae). Protoplasma. 2017;254:657–68.
75. Cao Y, Han Z, Zhang Z, He L, Huang C, Chen J, et al. UDP-glucosyltransferase 71C4 controls the flux of phenylpropanoid metabolism to shape cotton seed development. Plant Commun. 2024;5:100938.
76. Zhao Q, Lignification. Flexibility, biosynthesis and regulation. Trends Plant Sci. 2016;21:713–21.
77. Du J, Kirui A, Huang S, Wang L, Barnes WJ, Kiemle SN, et al. Mutations in the pectin methyltransferase QUASIMODO2 influence cellulose biosynthesis and wall integrity in Arabidopsis. Plant Cell. 2020;32:3576–97.

Publisher's note